The Authors would like to thank R2 for the helpful comments that helped to revise and improve the manuscript. Our replies are here in bold. Relevant changes in text and figures are illustrated at the end of this document, where added or modified text is highlighted in yellow.

1) This is an interesting MS showing the powerful application of LA-ICPMS for high resolution (200 um) ice core analysis. This may have a lot of implication especially for low accumulation sites and/or abrupt changes.

We are glad to see that R2 agrees with us that our cryo-cell LA-ICPMS methodology not only is powerful but also widely applicable.

2) There are some novelties in this paper on the way the authors prepared the standards to convert the count per seconds (intensities) into concentrations. However they use standard riverine waters (SLRS) and a suspension of NIST648 leached with ultrapure HNO3, which resulted in an ice matrix standard which is far from the real ice matrix. We know that the slopes of the calibration curves are highly dependent from the matrix itself and I think therefore that the results may be strongly biased by the different ionization of the ice matrix compared to the standard ones.

Ultimately we are ablating the same H_2O matrix in both samples and standards, so we respectfully disagree with R2 that they are 'far from the real ice matrix'. Using such artificial ice standards to calibrate LA-ICPMS analyses of ice goes back – with contrasting results as to the resultant homogeneity - to the pioneering work of Reinhard et al (2003), or Sneed et al. (2015). In fact, 193 nm excimer laser-ablation is known to be relatively more matrix-tolerant (Guillong et al., 2003) compared to other ns-LA methodology) such that, for example, *accurate* results can be obtained for as contrasting matrixes such as carbonate samples standardized with Na-Ca-Al-Si-glasses (the NIST61x glass suite). If available, we would appreciate a reference supporting the assertion 'We know that the slopes … are highly dependent from the matrix itself…', to be able to evaluate this ourselves.

However, we want to stress that our standardization is far from being perfect given the problem of making very homogenous ice stds. In the absence of a usable internal std (OH-signal is not sufficiently above background), this level of matrix-matching is actually state-of-the-art and thus the currently best available.

3) The authors should comment on this and clearly demonstrate how they obtain real concentration and not just relative changes that can be easily seen just looking at the variation of intensities.

All of our Ice standards were prepared by dilution between 1:10 and 1:1000 of the certified reference material with ultrapure H_2O (>18 MΩ·cm); we very mildly acidified these solutions with 1% ultrapure HNO_3 to stabilize them before freezing and to align them with the acidity of the multi-elemental standard solution ICP1 (Sigma-Aldrich), which was the only one being originally (before dilution) in 10% HNO_3, unlike all of our other standard solutions. We believe any bias introduced is contained within the ~ 16-

18 % error involved in the calibration procedure. This has been now clarified in the methodology section.

4) In addition, the authors claim to use 24Mg, 27Al, 40Ca, 56Fe. All these masses are highly interfered by spectral and matrix interferences in ICPMS. Despite I think they used a SF-ICP-MS or a collision-cell instrument to reduce the interferences, I think that a better description of the methodology should be given. I know that most of the details are given in Della Lunga (2014), but a minimal description of the methodology is compulsory.

We have added several details regarding the methodology, including a description of the removal of interferences by the use of H_2 in the Agilent 7500cs reaction cell; but we also note than these details are provided in our earlier publication in the Journal of Glaciology which had been included at the outset (Della Lunga et al., 2014). If the ice matrix was contributing to the signals on m/z=24, 27, 40, 56 then we would not obtain no resolvable counts from instrumental background for our ice blanks.

5) Then, I do not fully understand the objective of the MS, since most of the findings are not new at all. I would have rather focussed the MS into a comparison between LA-ICPMS vs CFA, but this would have required a more robust statistical tool.

I would therefore suggest the authors to readdress the MS to a specific target: i) analytical (in this case the paper lacks of many details), describing in detail the new advancement of this powerful technique and duly comparing the data with CFA results; in this case the reproducibility of the analysis on different sections is a key parameter, but as far as I can see there are no evidence of this in the paper; ii) more oriented toward a climatic/environmental interpretation; in this case the real benefit of the LA-ICP-MS approach should have been better explained.

As we also state in the reply to R1, the focus of the manuscript was predominantly methodological yet with one integral case study of deep ice to illustrate the power of the significantly improved, in fact unprecedented, spatial resolution. To make this focus clearer, the revised manuscript now presents a stronger methodological section and a more detailed description of the signal emerging from ablation with 193 nm laser and its possible interpretation. The climatic picture emerging from our analysis of GI21.2 is intended to demonstrate the capability of the technique to recover extremely small scale variability together with Stadial-Interstadial fingerprint in dust and sea salt proxies for one of the most abrupt and short lived transitions in deep ice where ice layer thickness is becoming very small.

Rerefences

Della Lunga, D., Müller, W., Rasmussen, S. O., & Svensson, A. (2014). Location of cation impurities in NGRIP deep ice revealed by cryo-cell UV-laser-ablation ICPMS. Journal of Glaciology, 60(223), 970-988.

Guillong, M., Horn, I., & Günther, D. (2003). A comparison of 266 nm, 213 nm and 193 nm produced from a single solid state Nd: YAG laser for laser ablation ICP-MS. Journal of analytical atomic spectrometry, 18(10), 1224-1230.

Reinhardt, H., Kriews, M., Miller, H., Lüdke, C., Hoffmann, E., & Skole, J. (2003). Application of LA–ICP–MS in polar ice core studies. Analytical and bioanalytical chemistry, 375(8), 1265-1275.

Sneed, S. B., Mayewski, P. A., Sayre, W. G., Handley, M. J., Kurbatov, A. V., Taylor, K. C. & Spaulding, N. E. (2015). New LA-ICP-MS cryocell and calibration technique for sub-millimeter analysis of ice cores. Journal of glaciology, 61(226), 233-242.

Post Review changes to:

Calibrated cryo-cell UV-LA-ICPMS elemental concentrations from NGRIP ice core reveal abrupt, sub-annual variability in dust across the interstadial period GI-21.2

Damiano Della Lunga[1], Wolfgang Müller[1], Sune Olander Rasmussen[2], Anders Svensson[2], Paul Vallelonga[2]
[1]Department of Earth Sciences, Royal Holloway University of London, Egham TW20 0EX, United Kingdom
[2]Centre for Ice and Climate, Niels Bohr Institute, University of Copenhagen, 2100 Copenhagen Ø, Denmark

Introduction

[……] This mechanism, which is thought to be the primary reason for sea-salt enrichment in ice cores during cooling events, receives further contributions of sea salt from another source. When sea ice is formed, highly saline brine and fragile frost flowers form on top of the frozen surface. This brine represents a further source of aerosol, carried over land by the wind (Wolff et al, 2003). However, a quantitative assessment of the contribution of brine, frost flowers, and blowing snow to the wintertime peak in sea salt aerosol it is still a matter of debate (Huang and Jaegle, 2016).

[……]The aim of the present study is to assess the sensitivity and the phasing of dust/sea-salt proxies as Na^{+}, Fe^{2+}, Al^{3+}, Ca^{2+} and Mg^{2+} at a resolution of ~200 µm (providing approximately 50 data points per calendar year at this depth) across the abrupt warming into and cooling out of the precursor event GI-21.2. Furthermore, we present an updated fully quantitative calibration for the elements under investigation, following Della Lunga et al. (2014) and Müller et al. (2011).

Methods and Calibration

This section corresponds to more than two hundred years, given the observed layer thickness of ~10 mm (Vallelonga et al., 2012). In the flow-model-based GICC05modelext timescale, the section covers an age range of 85.09 – 84.86 ka b2k and includes the 100-year long GI-21.2 and the transitions in and out of this period (Wolff et al., 2010; Rasmussen et al., 2014). We utilized samples from a similar position within the ice core cross section as in Della Lunga et al. (2014).

[……] The adopted methodology includes the acquisition of the following mass/charge ratios: 23(Na), 24(Mg), 27(Al), 34(S), 39(K), 40(Ca), 44(Ca), 55(Mn), 56(Fe), 65(Cu), 85(Rb), 88(Sr), 89(Y), 138(Ba), 139(La), 140(Ce), 141(Pr), 147(Sm), 153(Eu), 157(Gd), 172(Yb), 208(Pb), with dwell times ranging from 5 to 40 ms (see Della Lunga et al., 2014), and a total sweep time of 550 ms. Among these, only the following usually show resolvable signal/background ratio and will be displayed as results: 24(Mg), 27(Al), 40(Ca), 56(Fe). All elements were acquired in *reaction* mode, utilizing 4.5 ml/min of H_2 in the octopole cell, allowing the removal of conventional plasma interferences via charge transfer reaction, particularly significant on mass 40(Ca) and 56(Fe) from ^{40}Ar and $^{40}Ar^{16}O$. Mass 39(K), despite resolvable signal/background ratio, is affected by a potentially significant interference of ^{38}ArH resulting from adding H_2 in the reaction cell, and therefore will not be considered further. Formation of other hydrides has been monitored on specific isobaric-free masses (210, 233) in no gas and H_2 mode and resulted in no significant formation of such compounds in both cases. Rare Earth Elements were monitored as indicator of further possible contamination due to smoothing and were not the main target of this study.

[….] Each element has been externally calibrated using a set of four custom-made ice standards chosen from a total of five (SLRS-5, SLRS-5_10, ICP-20, NIST1648a and Water Low), prepared at RHUL from four different standard solutions at different concentrations and different dilutions (Table S1, see supplementary material). All of our Ice standards except SLRS-5 were prepared by dilution between 1:10 and 1:1000 of the certified reference material with ultrapure H_2O (>18 MΩ·cm); we very mildly acidified these solutions with 1% ultrapure HNO3 to stabilize them before freezing and to align them with the acidity of the multi-elemental standard solution ICP1 (Sigma-Aldrich), which was the only one being originally (before dilution) in 10% HNO_3, unlike all of our other standard solutions..

This external calibration assumes overall comparable ablation characteristics of NGRIP ice and ice standards, which in view of their similar matrix are a satisfactory assumption. Furthermore, using m/z=17 (OH) as an internal standard following Reinhardt et al. (2003), is not feasible because the significantly lower sample consumption of UV-LA relative to IR-LA (Müller et al., 2011) does not result in a background-resolved ICPMS signal at m/z=17.

[….] For each element, the slope of the equation of the regression line fitting all four standards in the linear plot has been calculated (together with the corresponding R^2 value) and utilized to convert net-intensities into concentrations. For the sake of display Fig. 4 show all the regression lines in a log-log plot.

Results

[….]Figures 9 and 10 show a collection of maps of calibrated concentrations of the elements under investigation from a 4x4 mm cross section at depth of 2689.78 and 2689.55 m. These sections were chosen specifically from depths were concentrations were high and presented a considerable degree of small scale variability as inferred from our laser ablation profiles.

LA-ICPMS-CFA data comparison

For comparison, our cryo-cell LA-ICPMS data have been plotted together in Fig 5-8 with previously published CFA results from the same NGRIP depths (Vallelonga et al., 2012). In contrast to the cryo-cell LA-ICPMS resolution of ~0.2 mm, the CFA profiles of Na, $\delta^{18}O$, CFA-dust and conductivity have a resolution of 3.5, 50, 1.5

and 1.5 mm respectively. The two datasets show some similarities: between a depth of 2691.50 and 2691.20 m the dust, and partly also the conductivity profiles present relatively high values, similar to what is observed for our elemental proxies, typical of the stadial GS-22 phase. At 2691.20 CFA-dust and LA data are both characterized by a decrease in concentrations, although the LA data show much clearer and abrupt features, marking the start of the GI-21.2 warm phase. Furthermore, minima for the entire section are located between depths of 2690.95 and 2690.15 m in both datasets. Also, both datasets agree in the shallowest part of the section, showing a more increasing trend starting at 2690.00 m.

In Fig.5, Na data from CFA and LA-ICPMS analyses have been plotted together on the same y-scale. The two datasets show overall analogous patterns in most of the section and in some sections broadly comparable average values, such as between 2690.00 – 2689.25 m (70 ppb and 67 ppb in the CFA and LA-ICPMS profile, respectively). However, LA-ICPMS-Na characteristically is more variable and differs from CFA data in the intervals 2689.20 – 2688.65 m and 2691.5 – 2691.5 m, where LA-ICPMS Na is either higher or lower relative to CFA-Na, respectively. This seems to indicate that there is not an overall systematic shift between the two techniques (see below). In general, the difference between LA-Na and CFA-Na, could derive from the tendency of Na to show higher concentrations in the proximity of grain boundaries and junctions, as it is described in the following section. Therefore, laser ablation tracks show much higher variability as a result of scanning across several boundaries and junctions at small scale, introducing a factor of differentiation that is also reflected in our calibration since it reduces the homogeneity of our ice standards.

As a further test, we compared the cryo-cell UV-LA-ICPMS data acquired in the frozen state with results from the same three NGRIP samples analysed via solution-ICPMS after melting (10 ml). The three samples correspond to three different depths in the immediate vicinity of GI-21.2 and representing a wide range of concentrations: early GS-22 (sample 4940A11), late GS-22 (sample 4900A3) and GI-21.1 (sample 4882B4). Results show that calibrated solution data are consistent with our LA-ICPMS data and differ by 5 – 20 %, which is essentially within our margin of error. Sample 4882B4, representing the last part of GS-21.2, shows the lowest concentrations amongst the three samples and also the consistently largest differences between solution and laser data (see Fig. S4 in the supplementary material).

Origin of Laser ablation elemental signal

The intensity of the LA-signal associated to a certain mass/charge ratio, characteristic to one element, is built up by two different contributions: one from soluble ions present in the ice matrix and the other one from dispersed insoluble mineral particles containing the element in their structure. Micro-particles in the NGRIP ice core have a mean grain size between 1 and 2 µm (Ruth et al., 2003) and therefore are too small to be identified unequivocally with our laser camera. Visual inspection of the sample before, after, and during ablation indicated that no residual spatter of the ablation process was deposited back onto the ice surface after the laser hit the sample, indicating a complete digestion of the material removed by the ablation pulses. This suggests that no fractionation between soluble and insoluble particle is taking place by effect of the laser sampling.

We investigated the spatial distribution of Na, Mg, Al, Ca and Fe over two small horizontal planes (i.e, perpendicular to the core length axis) by analysing 2D maps of concentrations across two of these specific cross sections (Fig 9 and 10). These sections were constructed interpolating several acquisition points obtained via static laser drilling. Fig 9 and 10 both show concentrations spanning over a range of several tens of ppb for each

element across the entire sections. The cross-sections intersect few grain boundaries and junctions (as observable in the laser camera image). The grain boundary net has been overlaid in black onto the elemental maps and shows that, in most of the cases, high concentrations areas are located in the proximity of boundaries and junction, broadly mimicking their pattern. In both cases, these patterns are somehow clearer for element like Na and Mg, related to sea salt, and become less defined going from Ca to Al and Fe. This might be associated with the fact that the elemental signal has a relative increasing contribution from micro-particles going from Ca to Al, to Fe, whereas the contribution from micro-particles to the Na and Mg signal would be minimal. This would also suggest that micro-particles are slightly less inclined to be aligned on boundaries and junctions compared to soluble impurities and therefore generate a less defined pattern of concentrations in our maps.

Discussion

[….] Most of the differences between CFA and LA-ICPMS proxies are observed at a small scale and are mainly influenced by few factors, the first of which is the effect of sample volume. In fact, we estimate that every LA-ICPMS data point corresponds to ~120 ng of ablated ice (based on scanning speed and ice crater depth) whereas CFA sampling resolution is about 0.1-1 g for each data point (Vallelonga et al., 2012). This introduces a difference in the sampling volume between the two datasets that can also be influenced by surface effects and especially by the wavy nature of layers at this scale and core depth. This is particularly important for Na, whose lateral variability induced by any non-horizontal layering is also affected by diffusion of Na that has been observed at this depth, resulting in a smoothing of the CFA annual signal (Vallelonga et al., 2012). Furthermore, the CFA insoluble dust data presented here refer to measurements of particles of size >1 μm and therefore do not account for insoluble impurities of sub-micron size (Vallelonga et al., 2012).

The elemental maps shown in Fig. 9 and 10 demonstrate that, at sub-cm scale, the concentrations of impurities it is strongly influenced by the presence of boundaries and junctions even when considering horizontal planes, whose original impurity-input is therefore assumed to be roughly identical. This introduces a main source of differentiation between LA and CFA sampling and can account for some of the small-scale variability we observe in the LA-profiles. This is particularly relevant for element like Na and Mg whose 2D distribution seems to follow closely the grain boundary net, presenting higher concentrations in the proximity of boundary and junction. On the other hand, 'dust'-proxies as Ca, Al and Fe, do not show such a closer overlap of high intensity and presence of boundaries or junctions, possibly as a result of being increasingly associated with insoluble micro-particles dispersed in the ice matrix, which indeed constitutes the CFA-Dust signal. This suggests that micro-particles in the ice matrix are less inclined to reside on boundaries and junction compared to soluble ions and is consistent with previous studies of deep ice cores (Della Lunga et al., 2014; Eichler et al., 2016). As a result, the averaging of LA-signal between two or more parallel tracks spaced by few mm is not only desirable but necessary.

Author contribution

DDL designed the experiment, performed the analysis, interpreted the data and wrote the manuscript. WM helped designing the experiment, performing the analysis and the data interpretation and edited the manuscript. SOR and AS contributed to the designing of the experiment, the sample preparation, the data interpretation and

edited the manuscript. PV provided CFA data for comparison, helped with the data interpretation and edited the manuscript.

Acknowledgements

This work has been supported by a RHUL studentship granted to Damiano Della Lunga, with the analytical costs being co-funded initially via a research grant from Resonetics LLC & Laurin Technic to Wolfgang Müller, and subsequently via a Postdoctoral grant from Australian Scientific Instruments (ASI) to both Damiano Della Lunga and Wolfgang Müller. The authors would like to thank Jerry Morris for continuing invaluable technical support at RHUL. Initial discussions with Michael Kriews and Dorothee Wilhelms-Dick helped to improve the methodology of ice standard preparation.

References

Barker, S., Chen, J., Gong, X., Jonkers, L., Knorr, G., & Thornalley, D. (2015). Icebergs not the trigger for North Atlantic cold events. Nature, 520(7547), 333-336.

Berglund, M., and Wieser, M. E. (2011). Isotopic compositions of the elements 2009 (IUPAC Technical Report). Pure and Applied Chemistry, 83(2), 397-410.

Bigler, M., Svensson, A., Kettner, E., Vallelonga, P., Nielsen, M. E., & Steffensen, J. P. (2011). Optimization of high-resolution continuous flow analysis for transient climate signals in ice cores. Environmental science & technology, 45(10), 4483-4489.

Boch, R., Cheng, H., Spötl, C., Edwards, R. L., Wang, X., and Häuselmann, P. (2011). NALPS: a precisely dated European climate record 120–60 ka. Climate of the Past, 7(4), 1247-1259.

Broecker, W., Bond, G., Klas, M., Clark, E., & McManus, J. (1992). Origin of the northern Atlantic's Heinrich events. Climate Dynamics, 6(3-4), 265-273.

Broecker, W. S. (2003). Does the trigger for abrupt climate change reside in the ocean or in the atmosphere?. Science, 300(5625), 1519-1522.

Capron, E., A. Landais, J. Chappellaz, A. Schilt, D. Buiron, Dahl-Jensen D., Johnsen S.J., Jouzel J., Lemieux-Dudon B., Loulergue L., Leuenberger M., Masson-Delmotte V., Meyer H., Oerter H., Stenni B. "Millennial and sub-millennial scale climatic variations recorded in polar ice cores over the last glacial period." Climate of the Past 6, 3 (2010): 345-365.

Clark, P. U., Pisias, N. G., Stocker, T. F., & Weaver, A. J. (2002). The role of the thermohaline circulation in abrupt climate change. Nature, 415(6874), 863-869.

Clement, A. C., Cane, M. A., & Seager, R. (2001). An Orbitally Driven Tropical Source for Abrupt Climate Change. Journal of Climate, 14(11), 2369-2375.

Clement, A. C., & Peterson, L. C. (2008). Mechanisms of abrupt climate change of the last glacial period. Reviews of Geophysics, 46(4).

Dansgaard, Willi, S. J. Johnsen, H. B. Clausen, D. Dahl-Jensen, N. S. Gundestrup, C. U. Hammer, C. S. Hvidberg, Steffensen J.P., Svelnbjornsdottir A.E., Jouzel J., Bond G.. (1993): "Evidence for general instability of past climate from a 250-kyr ice-core record." Nature, 364, no. 6434 218-220.

Della Lunga, D., Muller, W., Rasmussen, S. O., and Svensson, A. (2014). Location of cation impurities in NGRIP deep ice revealed by cryo-cell UV-laser-ablation ICPMS. Journal of Glaciology, 60(223).

Deplazes, G., Lückge, A., Peterson, L. C., Timmermann, A., Hamann, Y., Hughen, K. A., Röhl U., Laj C., Cane M. A., Sigman D.M., Haug, G. H. (2013). Links between tropical rainfall and North Atlantic climate during the last glacial period. Nature Geoscience, 6(3), 213-217.

Eichler, J., Kleitz, I., Bayer, M., Jansen, D., Kipfstuhl, S., Shigeyama, W., Weikusat, C., and Weikusat, I. (2016): Location and distribution of micro-inclusions in the EDML and NEEM ice cores using optical microscopy and in-situ Raman spectroscopy, The Cryosphere Discuss., in review.

Fuhrer, K., Wolff, E. W., and Johnsen, S. J. (1999). Timescales for dust variability in the Greenland Ice Core Project (GRIP) ice core in the last 100,000 years. Journal of Geophysical Research: Atmospheres (1984–2012), 104(D24), 31043-31052.

Gillette, D. A., and Passi, R. (1988). Modeling dust emission caused by wind erosion. Journal of Geophysical Research: Atmospheres (1984–2012), 93(D11), 14233-14242.

Grachev, A. M., Brook, E. J., Severinghaus, J. P., and Pisias, N. G. (2009). Relative timing and variability of atmospheric methane and GISP2 oxygen isotopes between 68 and 86 ka. Global Biogeochemical Cycles, 23(2).

Grootes, P. M., and Stuiver, M. (1997). Oxygen 18/16 variability in Greenland snow and ice with 10− 3-to 105-year time resolution. Journal of Geophysical Research: Oceans (1978–2012), 102(C12), 26455-26470.

Huang, J., & Jaeglé, L. (2016) Wintertime enhancements of sea salt aerosol in polar regions consistent with a sea-ice source from blowing snow. *Atmospheric Chemistry and Physics*, in review.

Huber, C., Leuenberger, M., Spahni, R., Fluckiger, J., Schwander, J., Stocker, T. F.,Johnsen S., Landais A., Jouzel, J. (2006). Isotope calibrated greenland temperature record over marine isotope stage 3 and its relation to CH4. Earth and Planetary Science Letters, 243(3-4), 504-519.

Jochum, K. P., Weis, U., Stoll, B., Kuzmin, D., Yang, Q., Raczek, I., Jacob D.E., Stracke A., Birbaum K., Frick D. A., Günther D., and Enzweiler, J. (2011). Determination of reference values for NIST SRM 610–617 glasses following ISO guidelines. Geostandards and Geoanalytical Research, 35(4), 397-429.

Johnsen, S. J., Clausen, H. B., Dansgaard, W., Fuhrer, K., Gundestrup, N., Hammer, C. U., Iversen P., Jouzel J., Stauffer B., Steffensen, J. P. (1992). Irregular glacial interstadials recorded in a new Greenland ice core. Nature, 359(6393), 311-313.

Kreutz, K.J., and Koffman, B., (2013), Glaciochemistry, in Encyclopedia of Quaternary Science 2nd edition, S. Elias, ed., Elsevier Publishers, 326-333.

Kutzbach, J. E., Guetter, P. J., Behling, P. J., and Selin, R. (1993). Simulated climatic changes: results of the COHMAP climate-model experiments. Global climates since the last glacial maximum, 24-93.

Lewis, E. R., & Schwartz, S. E. (2004). Sea salt aerosol production: mechanisms, methods, measurements, and models-A critical review. American Geophysical Union, 2004.

MacAyeal, D. R. (1993). Binge/purge oscillations of the Laurentide ice sheet as a cause of the North Atlantic's Heinrich events. Paleoceanography, 8(6), 775-784.

Mahowald, N., Kohfeld, K., Hansson, M., Balkanski, Y., Harrison, S. P., Prentice, I. C., Schulz M., Rodhe, H. (1999). Dust sources and deposition during the last glacial maximum and current climate: A comparison of model results with paleodata from ice cores and marine sediments. Journal of Geophysical Research: Atmospheres, 104(D13), 15895-15916.

Masson-Delmotte, V., Jouzel J., Landais A., Stievenard M., Johnsen S.J., White J. W. C., Werner M., Sveinbjornsdottir A., Fuhrer K (2005). "GRIP deuterium excess reveals rapid and orbital-scale changes in Greenland moisture origin." Science 309, no. 5731 (2005): 118-121.

Müller, W., Shelley, M., Miller, P., and Broude, S. (2009). Initial performance metrics of a new custom-designed ArF excimer LA-ICPMS system coupled to a two-volume laser-ablation cell. Journal of Analytical Atomic Spectrometry, 24(2), 209-214.

Müller, W., Shelley, J. M. G., and Rasmussen, S. O. (2011). Direct chemical analysis of frozen ice cores by UV-laser ablation ICPMS. Journal of Analytical Atomic Spectrometry, 26(12), 2391-2395.

Petersen, S. V., Schrag, D. P., & Clark, P. U. (2013). A new mechanism for Dansgaard-Oeschger cycles. Paleoceanography, 28(1), 24-30.

Petit, J. R., Jouzel, J., Raynaud, D., Barkov, N. I., Barnola, J. M., Basile, I, M. Bender, J., Chappellaz, M. Davis, G. Delaygue, M. Delmotte, V. M. Kotlyakov, M. Legrand, V. Y. Lipenkov, C. Lorius, L. PÉpin, C. Ritz, E. Saltzman and Stievenard, M. (1999). Climate and atmospheric history of the past 420,000 years from the Vostok ice core, Antarctica. Nature, 399(6735), 429-436.

Randall, D.A., R.A. Wood, S. Bony, R. Colman, T. Fichefet, J. Fyfe, V. Kattsov, A. Pitman, J. Shukla, J. Srinivasan, R.J. Stouffer, A. Sumi and K.E. Taylor, (2007). Climate Models and Their Evaluation. In: Climate Change 2007: The Physical Science Basis. Contribution of Working Group I to the Fourth Assessment Report of the Intergovernmental Panel on Climate Change [Solomon, S., D. Qin, M. Manning, Z. Chen, M. Marquis, K.B. Averyt, M.Tignor and H.L. Miller (eds.)]. Cambridge University Press, Cambridge, United Kingdom and New York, NY, USA.

Rasmussen, S. O., Bigler, M., Blockley, S. P., Blunier, T., Buchardt, S. L., Clausen, H. B. and Winstrup, M. (2014). A stratigraphic framework for abrupt climatic changes during the Last Glacial period based on three synchronized Greenland ice-core records: refining and extending the INTIMATE event stratigraphy. Quaternary Science Reviews. volume 106, 14–28.

Reinhardt, H., Kriews, M., Miller, H., Lüdke, C., Hoffmann, E., & Skole, J. (2003). Application of LA–ICP–MS in polar ice core studies. Analytical and bioanalytical chemistry, 375(8), 1265-1275.

Ruth, U., Wagenbach, D., Steffensen, J. P., & Bigler, M. (2003). Continuous record of microparticle concentration and size distribution in the central Greenland NGRIP ice core during the last glacial period. Journal of Geophysical Research: Atmospheres, 10.

Seierstad, I. K., Abbott, P. M., Bigler, M., Blunier, T., Bourne, A. J., Brook, E., Buchardt S. L., Buizert C., Clausen H. B., Cook E., Dahl-Jensen D.,. Davies S. M., Guillevic M., Johnsen S. J., Pedersen D. S., Popp T. J, Rasmussen S. O., Severinghaus J. P., Svensson A. & Vinther, B. M. (2014). Consistently dated records from the Greenland GRIP, GISP2 and NGRIP ice cores for the past 104 ka reveal regional millennial-scale δ 18 O gradients with possible Heinrich event imprint. Quaternary Science Reviews, 106, 29-46.

Severinghaus, J. P., and Brook, E. J. (1999). Abrupt climate change at the end of the last glacial period inferred from trapped air in polar ice. Science, 286(5441), 930-934.

Sneed, S. B., Mayewki, P. A., Sayre, W., Handley, M. J., Kurbatov, A. V., Taylor, K. C., Bohleber P., Wagenbach D., Erhardt T., Spaulding, N. E. (2015). Instruments and Methods New LA-ICP-MS cryocell and calibration technique for sub-millimeter analysis of ice cores. Journal of Glaciology, 61(226), 233.

Spötl, C., & Mangini, A. (2002). Stalagmite from the Austrian Alps reveals Dansgaard–Oeschger events during isotope stage 3: Implications for the absolute chronology of Greenland ice cores. Earth and Planetary Science Letters, 203(1), 507-518.

Steffensen, J. P., Andersen, K. K., Bigler, M., Clausen, H. B., Dahl-Jensen, D., Fischer, H., Goto-Azuma K., Hansson M., Johnsen S. J., Jouzel J., Masson-Delmotte V., Popp T.,. Rasmussen S. O, R. Röthlisberger R., Ruth

U., Stauffer B., Siggaard-Andersen M. L., Sveinbjörnsdóttir Á. E., Svensson A.,. White, J. W. C. (2008). High-resolution Greenland ice core data show abrupt climate change happens in few years. Science, 321(5889), 680-684.

Stocker, T.F., D. Qin, G.-K. Plattner, L.V. Alexander, S.K. Allen, N.L. Bindoff, F.-M. Bréon, J.A. Church, U. Cubasch, S. Emori, P. Forster, P. Friedlingstein, N. Gillett, J.M. Gregory, D.L. Hartmann, E. Jansen, B. Kirtman, R. Knutti, K. Krishna Kumar, P. Lemke, J. Marotzke, V. Masson-Delmotte, G.A. Meehl, I.I. Mokhov, S. Piao, V. Ramaswamy, D. Randall, M. Rhein, M. Rojas, C. Sabine, D. Shindell, L.D. Talley, D.G. Vaughan and S.-P. Xie, 2013: Technical Summary. In: Climate Change 2013: The Physical Science Basis. Contribution of Working Group I to the Fifth Assessment Report of the Intergovernmental Panel on Climate Change [Stocker, T.F., D. Qin, G.-K. Plattner, M. Tignor, S.K. Allen, J. Boschung, A. Nauels, Y. Xia, V. Bex and P.M. Midgley (eds.)]. Cambridge University Press, Cambridge, United Kingdom and New York, NY, USA, pp. 33–115,

Svensson, A., Nielsen, S. W., Kipfstuhl, S., Johnsen, S. J., Steffensen, J. P., Bigler, M., Ruth, U., Rothlisberger, R. (2005). Visual stratigraphy of the north Greenland ice core project (NorthGRIP) ice core during the last glacial period. Journal of Geophysical Research-Atmospheres,110(D2), D02108.

Thomas, E. R., Wolff, E. W., Mulvaney, R., Johnsen, S. J., Steffensen, J. P., and Arrowsmith, C. (2009). Anatomy of a Dansgaard-Oeschger warming transition: High-resolution analysis of the north Greenland ice core project ice core. Journal of Geophysical Research-Atmospheres, 114, D08102.

Vallelonga, P., Bertagna, G., Blunier, T., Kjaer, H. A., Popp, T. J., Rasmussen, S. O., Stowasser C., Svensson A. S., Winstrup M., Kipfstuhl, S. (2012). Duration of Greenland stadial 22 and ice-gas Δage from counting of annual layers in Greenland NGRIP ice core. Climate of the Past Discussions, 8(4), 2583-2605.

Voelker, A. H. (2002). Global distribution of centennial-scale records for Marine Isotope Stage (MIS) 3: a database. Quaternary Science Reviews, 21(10), 1185-1212.

Wang, Y. J., Cheng, H., Edwards, R. L., An, Z. S., Wu, J. Y., Shen, C. C., & Dorale, J. A. (2001). A high-resolution absolute-dated late Pleistocene monsoon record from Hulu Cave, China. Science, 294(5550), 2345-2348.

Wilhelm-Dick, D. (2008). Enhanced analysis of stratified climate archives through upgrade of Laser Ablation Inductively Coupled Plasma Quadrupole to Time of Flight Mass Spectrometry? (Doctoral dissertation, Berlin, Univ., Diss.).

Wolff, E. W., Rankin, A. M., and Röthlisberger, R. (2003). An ice core indicator of Antarctic sea ice production? Geophysical Research Letters, 30(22).

Wolff, E. W., Chappellaz, J., Blunier, T., Rasmussen, S. O., & Svensson, A. (2010). Millennial-scale variability during the last glacial: The ice core record. Quaternary Science Reviews, 29(21), 2828-2838.

Yung, Y. L., Lee, T., Wang, C. H., & Shieh, Y. T. (1996). Dust: A diagnostic of the hydrologic cycle during the Last Glacial Maximum. Science, 271(5251), 962-963.

Zhang, X. Y., Arimoto, R., & An, Z. S. (1997). Dust emission from Chinese desert sources linked to variations in atmospheric circulation. Journal of Geophysical Research. D. Atmospheres, 102, 28-041.

Zhang, X., Lohmann, G., Knorr, G., & Purcell, C. (2014). Abrupt glacial climate shifts controlled by ice sheet changes. Nature. 512, 290–294

Figures Captions

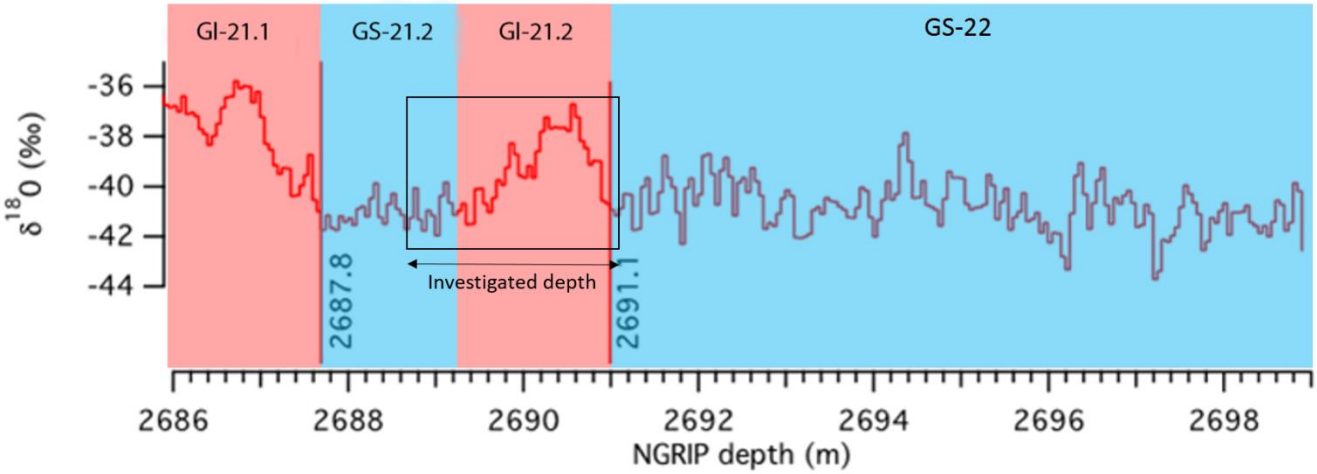

Figure 1: $\delta^{18}O$ profile across the transition from GS-22 to GI-21.1 (modified from Vallelonga et al., 2012). Stadial and interstadial periods are highlighted in blue and red, respectively. The black box and arrow indicate the corresponding section of ice core analysed for this study.

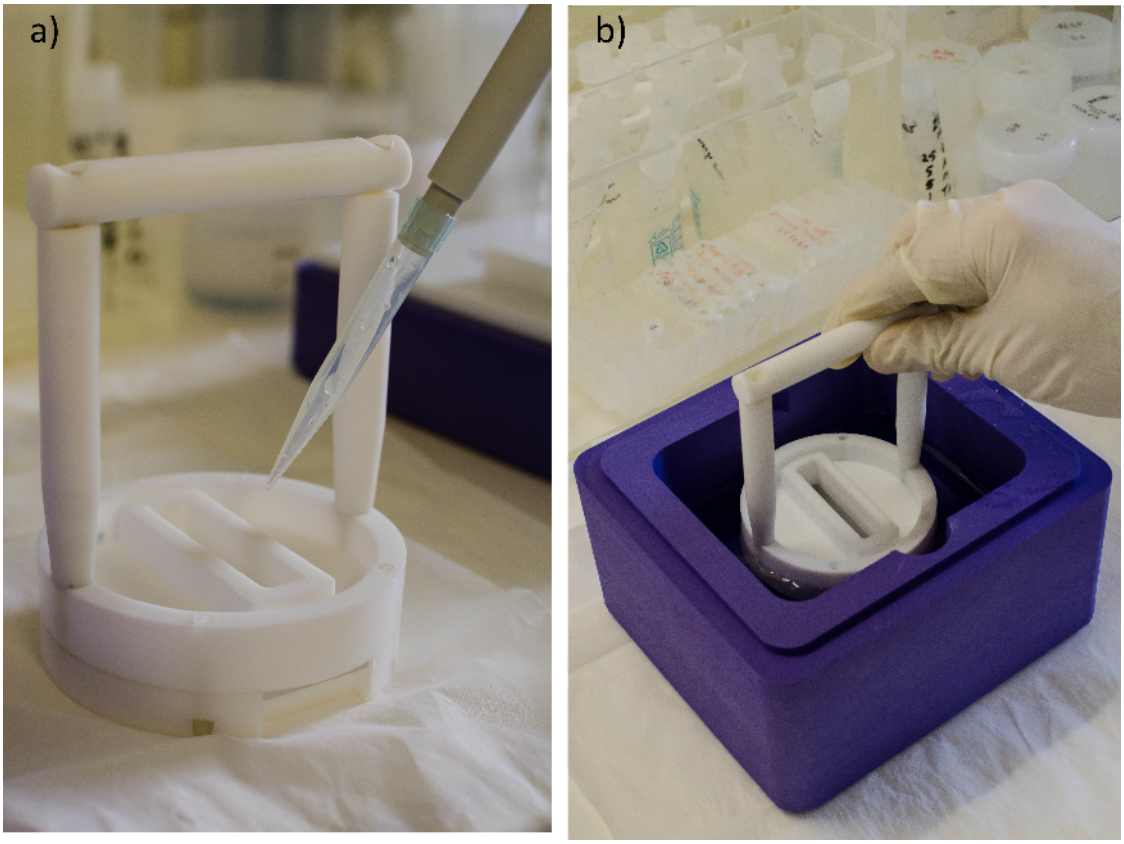

Figure 2: Ice standard preparation at RHUL. a) 1 ml of aqueous standard solution is pipetted into the inner volume of a PTFE mould featuring a removable glass surface at the bottom to allow the solution to spread uniformly creating a thin layer of water. b) The mould is dipped into liquid nitrogen to instantaneously shock-freeze the solution. This procedure is repeated five times to build up an ice volume by shock-freezing layer by layer of 5 ml total volume resulting in an ice volume approximately 45x10x10 mm. Each ice standard was then surface-cleaned using our PTFE vice before analysis (see text).

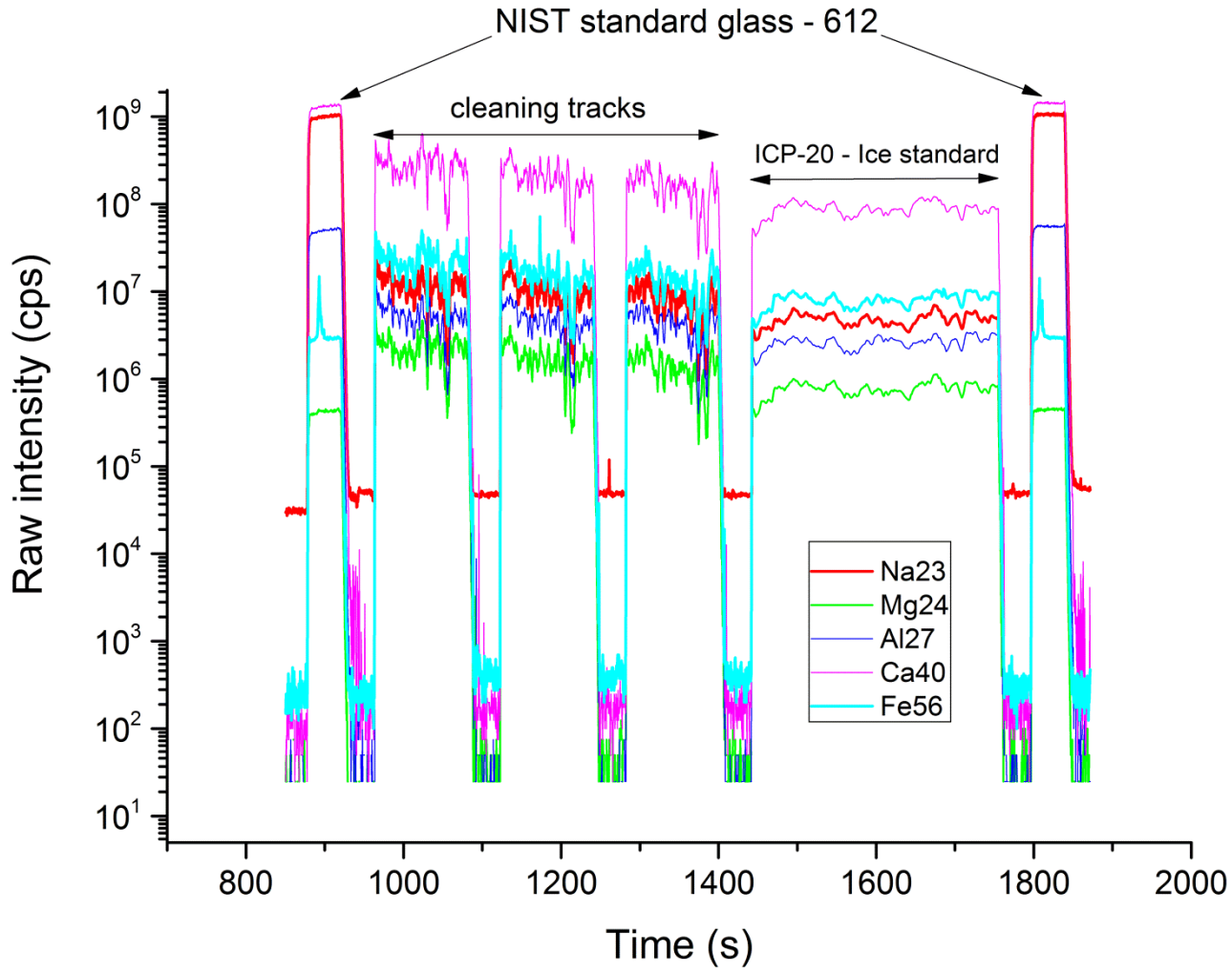

Figure 3: Example of raw intensity data of NIST612 glass (first and last peak) compared to one of the ice standards prepared for this study (ICP-20). Standard data were acquired following three cleaning runs, and show that the ice standard appears rather homogeneous with typical RSD values between ± 10 and 15 %. See text for details.

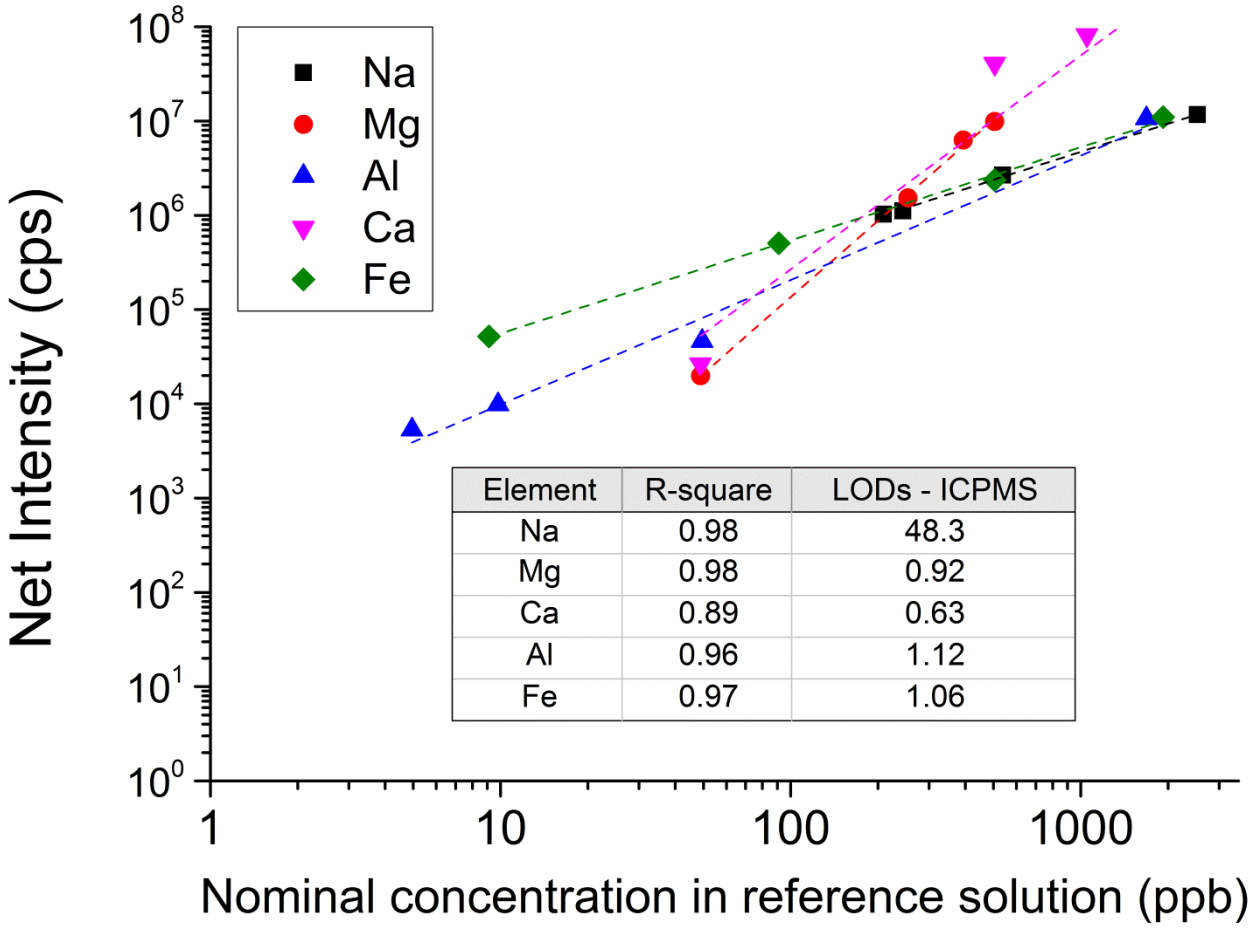

Figure 4: Calibration lines for elements under investigation obtained utilizing the ice standards listed in Table S1 (supplementary material). LOD indicates limits of detection. See text for details.

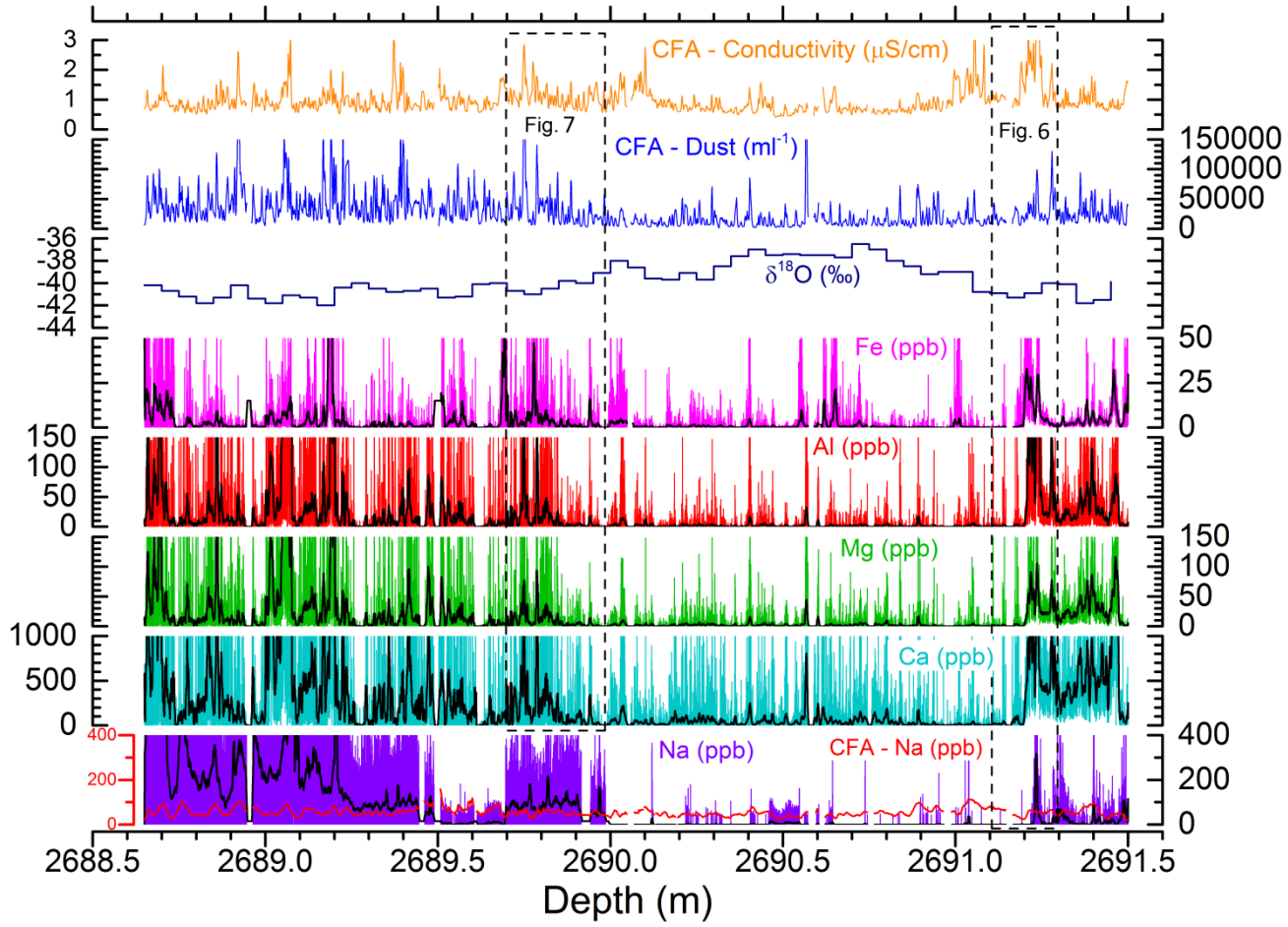

Figure 5: Cryo-cell-LA-ICPMS element concentration profiles of Na, Mg, Al, Ca, and Fe and corresponding Na, $\delta^{18}O$ and CFA-dust profiles at 3.5, 50 and 1.5 mm resolution respectively (the latter three from Vallelonga et al., 2012) across 2.85 m of NGRIP ice core that spans from approximately 85090 to 84860 a b2k (±20 a) and contains GI-21.2. The coloured lines are individual LA-ICPMS data points; black lines represent adjacent-element moving average (period 200). It should be noted that cryo-cell-LA-ICPMS Na LOD is 48.3 ppb, which renders most of the interstadial and some stadial Na data undetectable. Overall, Na is mainly shown to allow some comparability with existing CFA Na data (Vallelonga et al., 2012). See text for details.

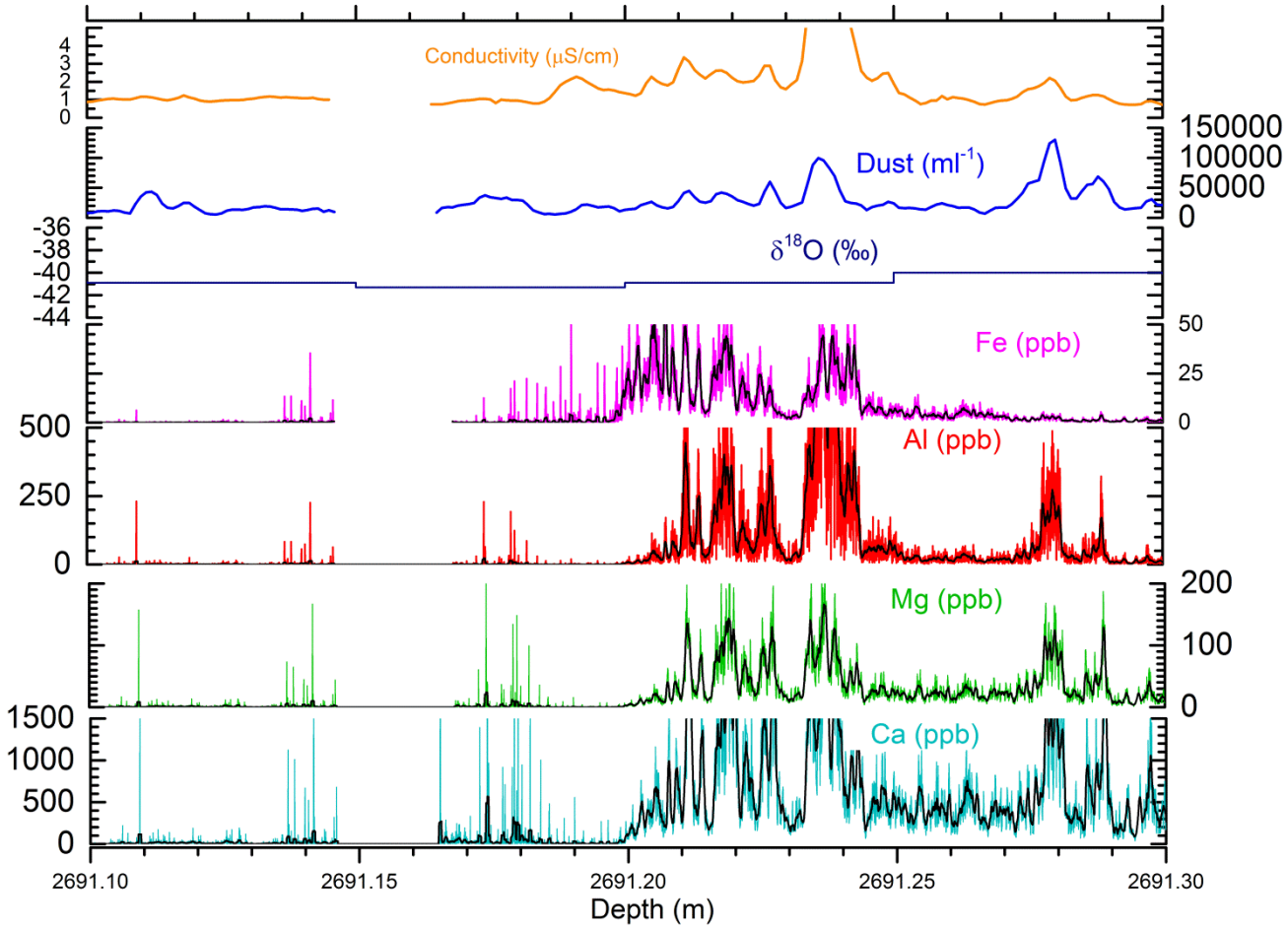

Figure 6: Zoomed-in cryo-cell LA-ICPMS profiles of a 200 mm window from the deepest part of the GI-21.2 section (cold/warm transition), analysed for the most significant elements and spanning about two decades around 85.1 ka b2k. Coloured lines represent LA data, black lines are 30-points moving averages. A switch between stadial and interstadial typical concentrations is observable around 2691.20 m, happening over the space of just ~10 mm. Conductivity and CFA-dust are from Vallelonga et al. (2012).

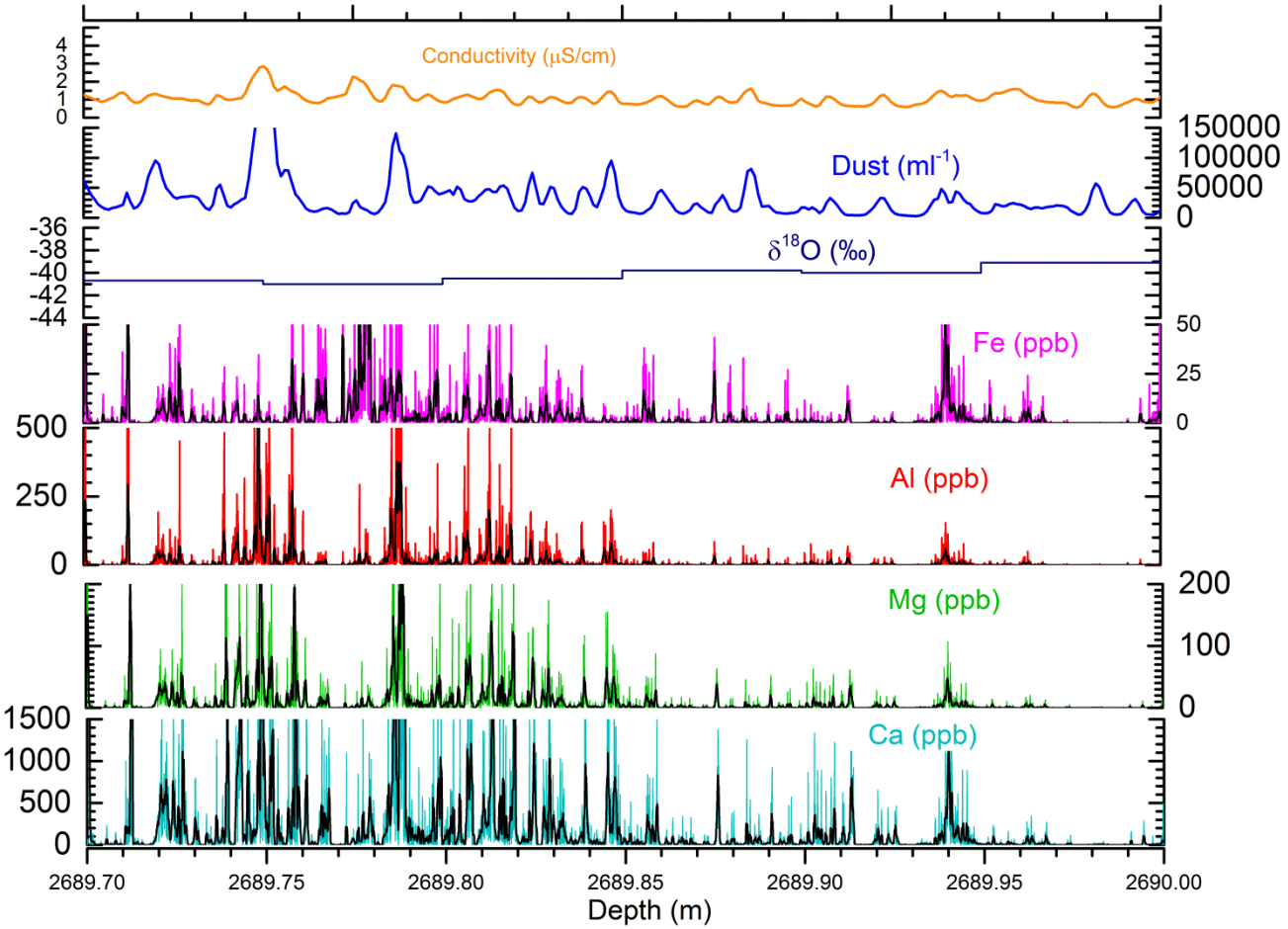

Figure 7: Zoomed-in cryo-cell LA-ICPMS profiles of a 300 mm window from the middle part of the GI-21.2 section analysed for the most significant elements and spanning about two decades around 85.0 ka b2k (cold-warm transition). Coloured lines represent LA data, black lines are 30-points moving averages. A gradual increase in dustiness is observable starting from a depth of 2689.95 m going towards shallower depths, representing the GI-21.2 – GS-21.2 transition, which in this case takes place over the space of ~150 mm. Conductivity and CFA-dust are from Vallelonga et al. (2012).

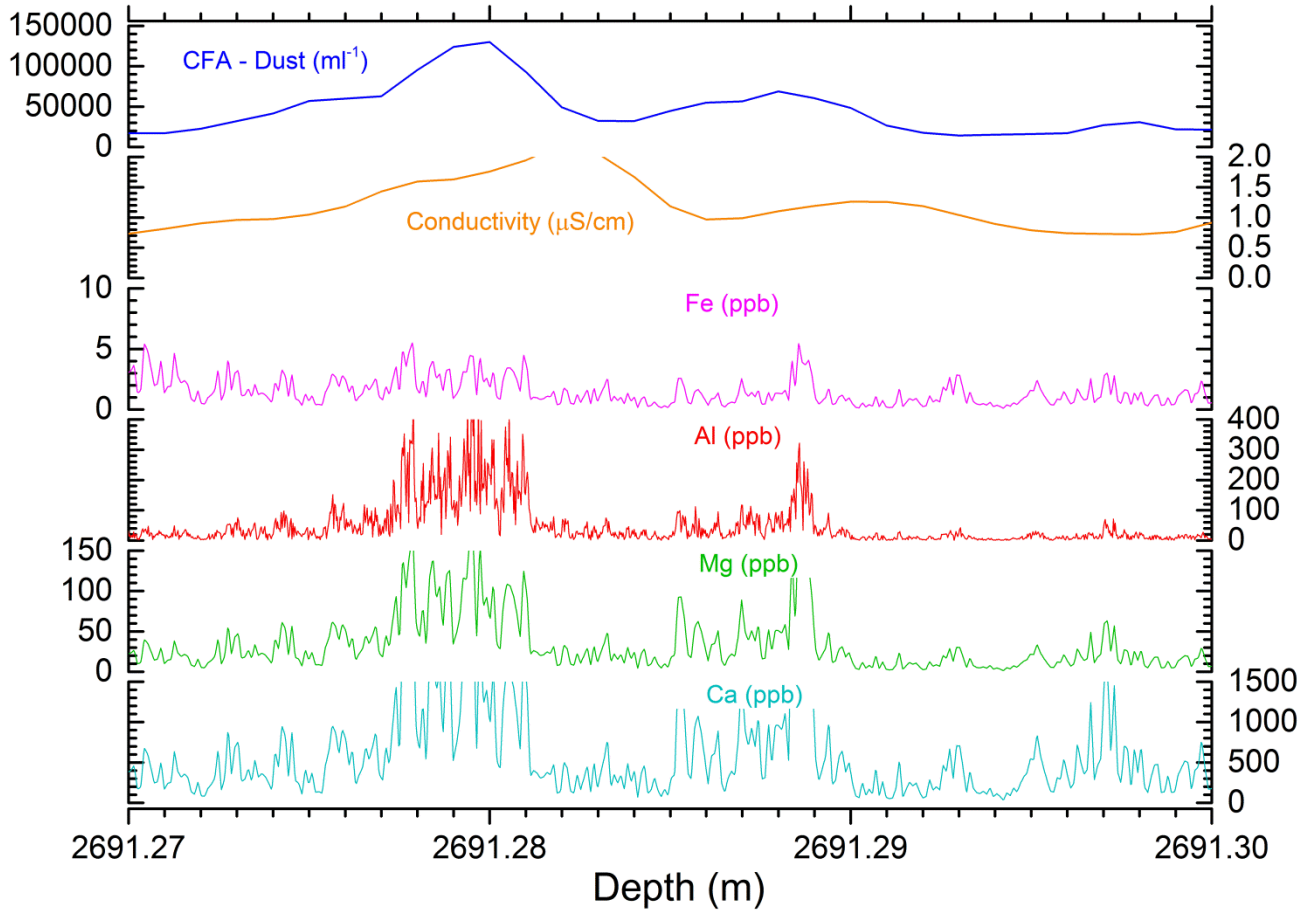

Figure 8: CFA conductivity, CFA dust, LA-Fe, LA-Ca, LA-Al and LA-Mg direct comparison across a detailed 3-cm zoom. In this case, laser ablation data have not been smoothed. Conductivity and CFA-dust are from Vallelonga et al. (2012). The profiles show sub-annual variations that contribute to the CFA annual signal.

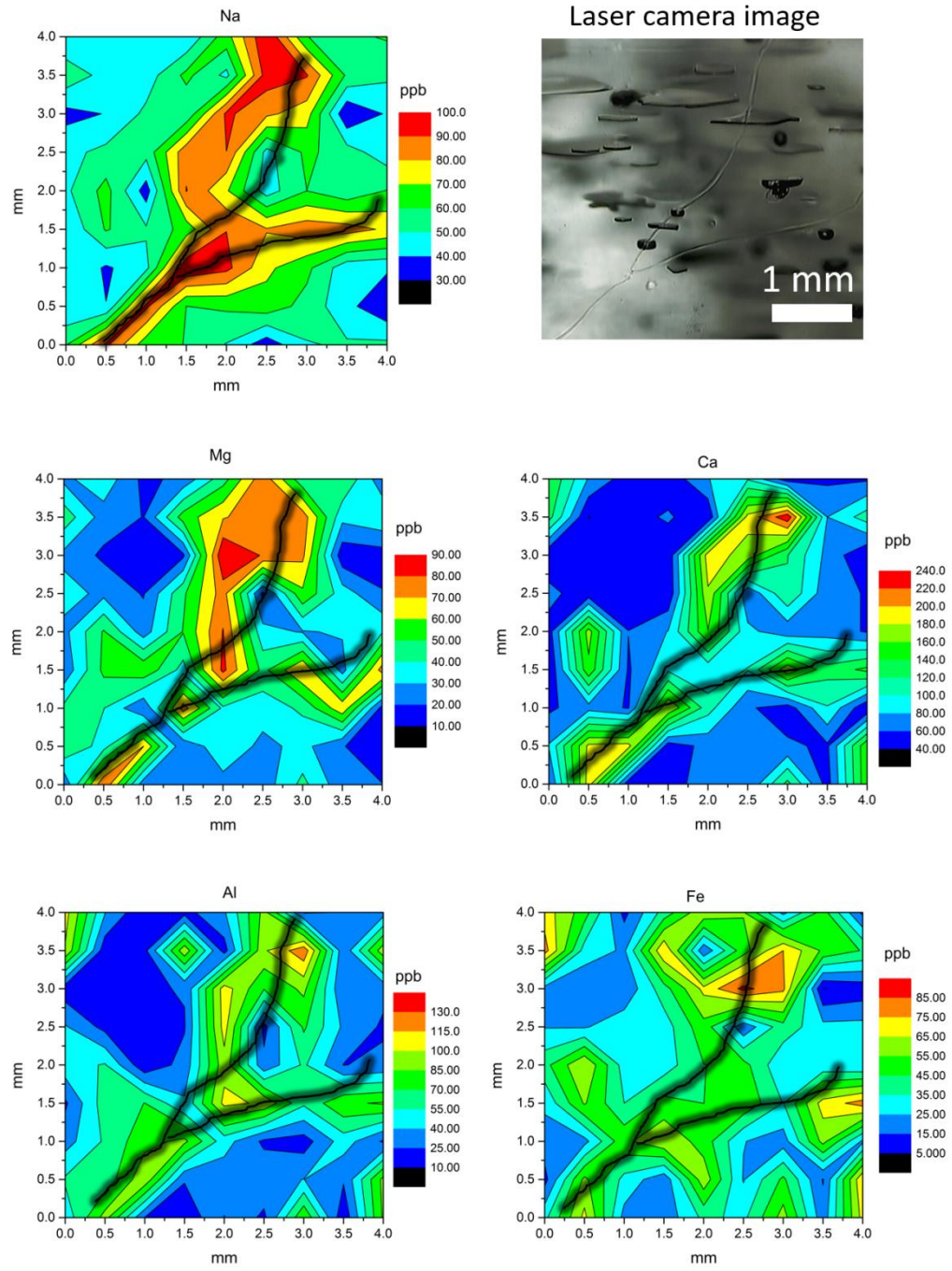

Figure 9: 2D maps of calibrated concentrations of elements under investigation (Na, Mg, Ca, Al, Fe) across a 4x4 mm cross section with overlaid grain boundary net in black as observed in transmitted light (upper right) from a depth of 2689.78 m.

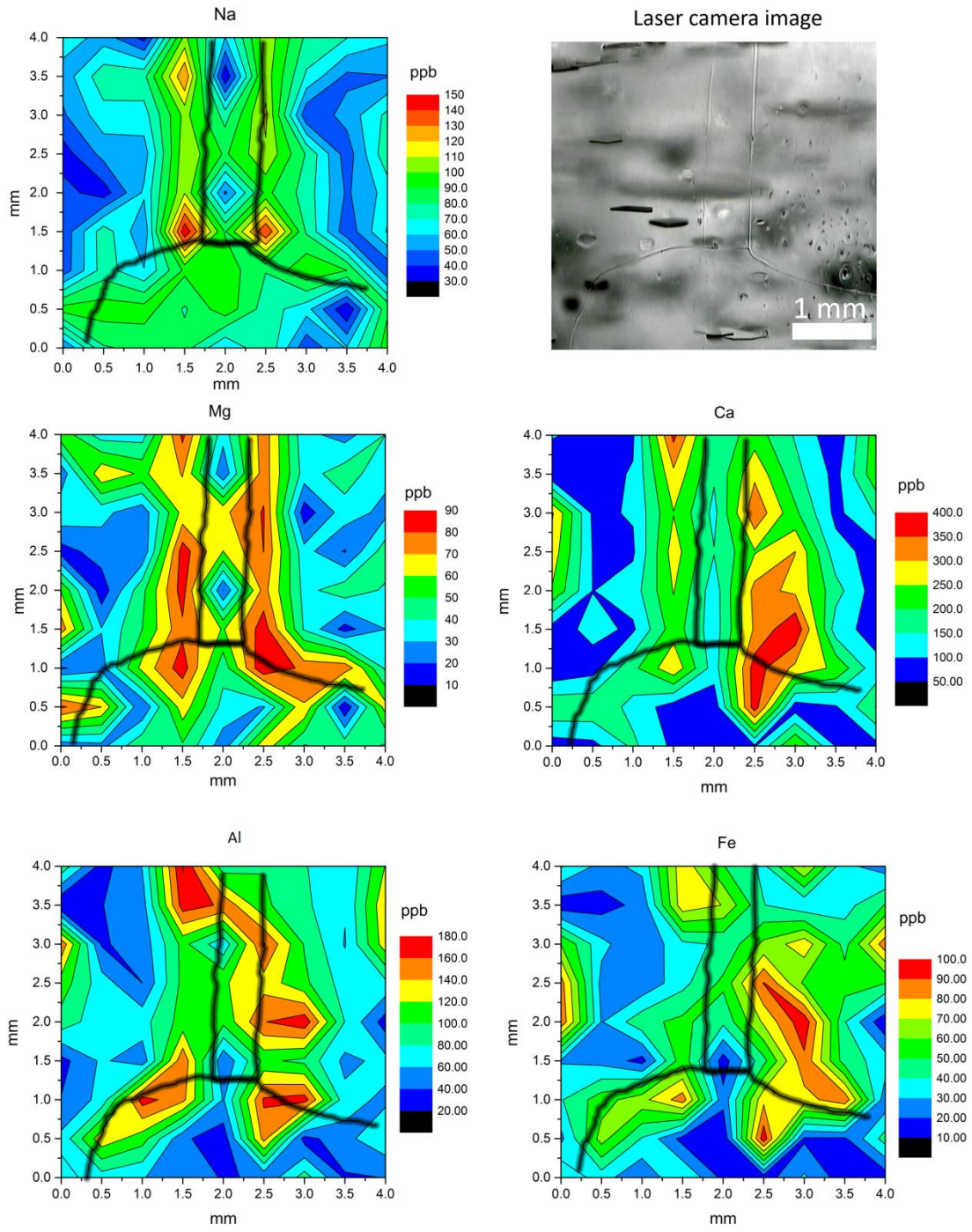

Figure 10: 2D maps of calibrated concentrations of elements under investigation (Na, Mg, Ca, Al, Fe) across a 4x4 mm cross section with overlaid grain boundary net in black as observed in transmitted light (upper right) from a depth of 2689.65 m.

Supplementary material

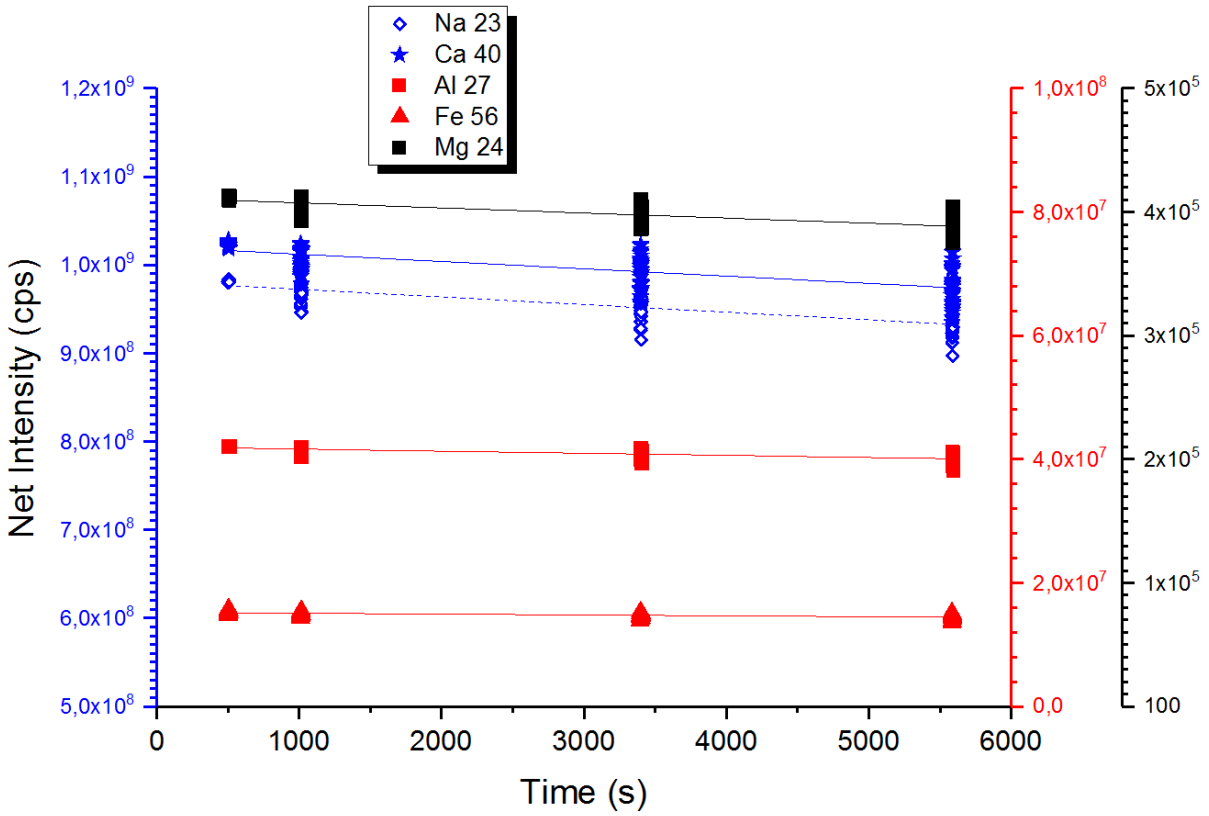

Figure S1: LA-ICPMS instrumental drift correction. The data points represent NIST612 values acquired in between the ice samples during a single run (axes are color-coded). Sensitivity typically decreases slightly during the analysis and the slope of each element's regression line has been utilized to correct instrumental drift according to eq.1 (See text for details).

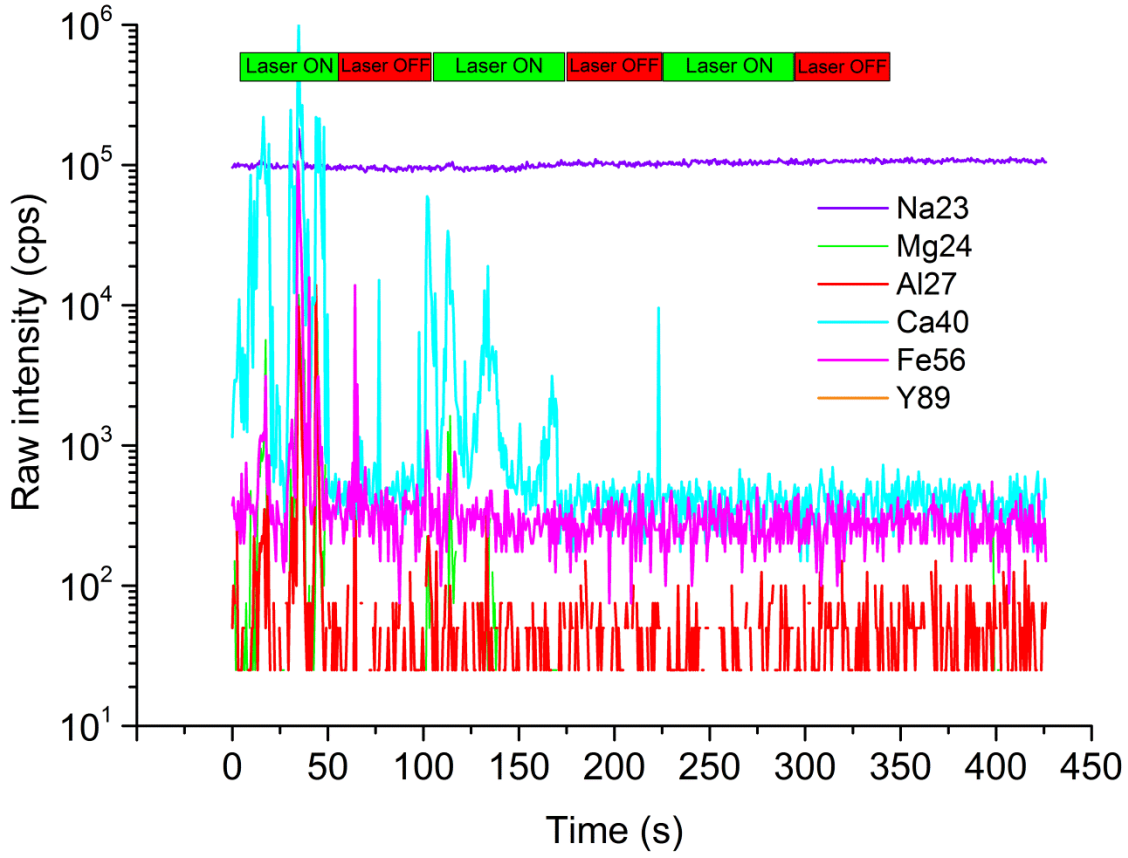

Figure S2: UV-LA-ICPMS analysis of an ice blank. The analysis includes three passages of the laser with 280 µm spot size, 25 Hz repetition rate and 8 mm/min speed, while the last acquisition track has been performed with 212 µm spot size, 20 Hz repetition rate and 3 mm/min speed where no analytes are above ICPMS background anymore. Analytes are the most abundant isotopes for each element. Table 1 lists the calibrated concentration (in ppb) of the major elements under investigation in the ultrapure water utilized to create ice blanks. See text for details.

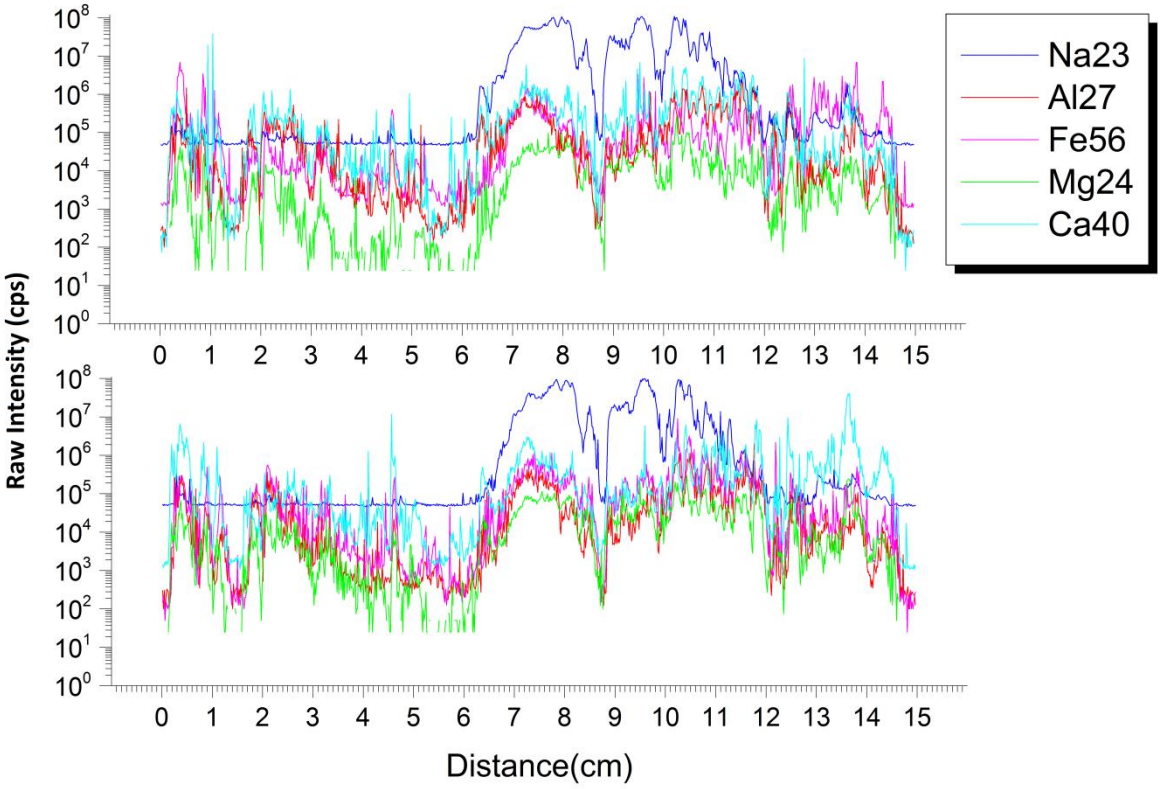

Figure S3: Reproducibility of LA tracks: example of raw intensities (cps) of main elements from 2 mm apart parallel ablation tracks acquired over 15 cm (3 samples) between depths of 2691.45-2691.30 m (left to right).

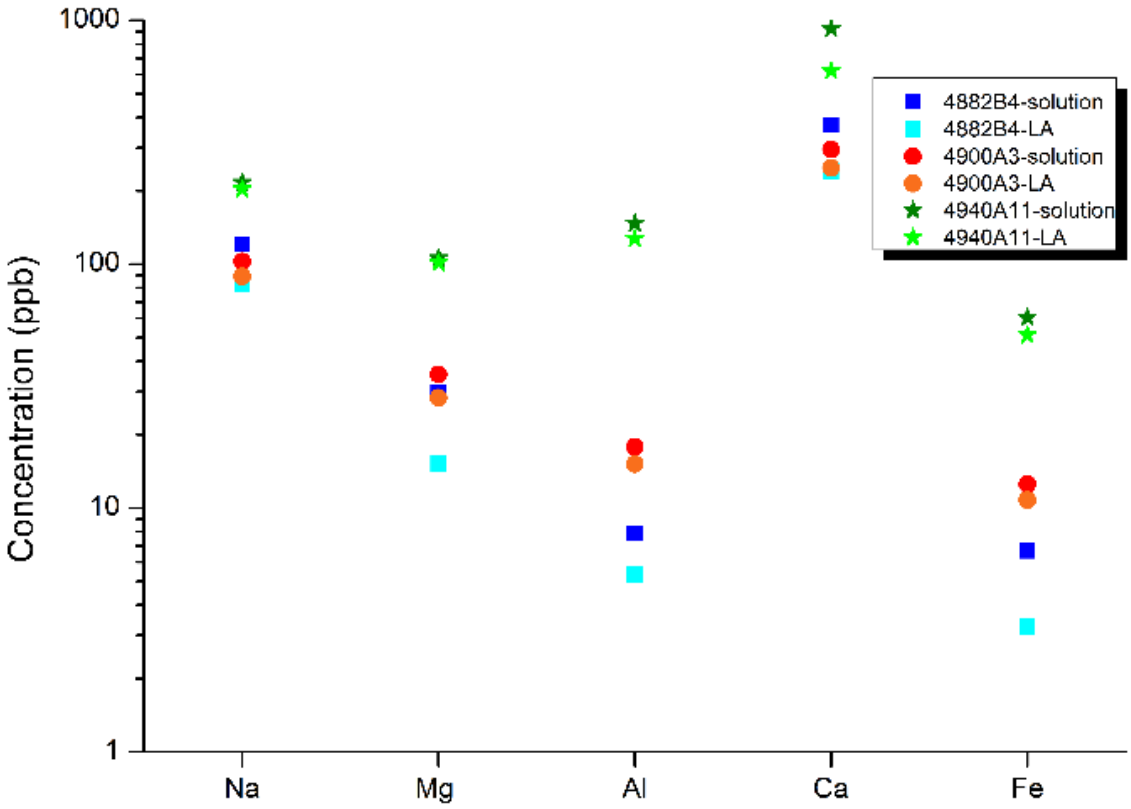

Figure S4: Comparison between solution data and cryo-cell UV-LA-ICPMS data on three different samples corresponding to three different 50-mm depth intervals: 4940A11 (depth range: 2716.45 – 2716.50 m), 4900A3 (depth range: 2694.85 – 2694.90 m) and 4882B4 (depth range: 2684.875 – 2684.925 m), representing small sections of early GS-22, late GS-22 and GI-21.1, respectively. Results show that LA and solution data differ of only 5 – 20% and therefore are within error margins. See text for details.

Table S1: Concentration of elements under investigation in aqueous reference materials used for ice standard preparation: SLRS-5-"River water reference material for trace metals" (National Research Council of Canada, diluted 10 times [SLRS-5_10] when not specified), Water low (RHUL internal standard), 90243 Multi-element standard solution 1 for ICP (Sigma Aldrich, diluted 20 times), and NIST SRM 1648 Urban Particulate reference material (in suspension, see text for details). Blank concentrations (in ppb) of ultrapure water at RHUL were obtained in solution mode and are shown on the right column. Limit of detection (LOD) refer to cryo-cell LA-ICPMS analyses only.

	Standard name					
	SLRS-5_10	ICP-20	Water Low	NIST1648a		RHUL Deionized water
Element	**concentration (ppb)**	**concentration (ppb)**	**concentration (ppb)**	**concentration (ppb)**	**LODs LA-ICPMS (ppb)**	**(ppb)**
Al	4.95 ± 0.5 49.5 ± 4.8 (SLRS-5)	2525±2.5	9.8±0.1	1683±16	1.12	0.012
Fe	9.1 ± 0.6 91 ±6 (SLRS-5)	505±0.5	9.8±0.1	1924±20	1.06	0.627
Ca	1050 ± 40 10510±380 (SLRS-5)	505±0.5	48.9±0.3	3126±15	0.63	0.606
Mg	254 ± 16 2541±155 (SLRS-5)	505±0.5	48.9±0.3	394±5	0.92	0.021
Na	538 ± 10 5380±105 (SLRS-5)	2525±2.5	244±1.5	209±4	48.3	-